2.N

Nuclear Physics **A299** (1978) 321–332; © *North-Holland Publishing Co., Amsterdam*

Not to be reproduced by photoprint or microfilm without written permission from the publisher

MICROSCOPIC AND PROXIMITY NUCLEUS-NUCLEUS POTENTIALS

D. M. BRINK

Theoretical Physics Department, 1 Keble Road, Oxford, UK

and

Fl. STANCU

Institut de Physique, Université de Liège, Sart Tilman, B-4000 Liège 1, Belgium
and
Nuclear Physics Department, Keble Road, Oxford, UK

Received 27 December 1977

Abstract: The energy functional of the Skyrme interaction is employed to calculate the real part of the interaction potential between magic nuclei in the sudden approximation. The use of an approximation introduced by Kirzhnits and others for the kinetic energy density produces improvements over the previous results. The mass dependence of the potential is analysed and its consistency with the proximity potential is discussed.

1. Introduction

The Skyrme interaction energy functional [1]) provides a convenient basis for the calculation of the interaction potential between two nuclei. In static calculations several methods have been employed: the self-consistent method [2–4]), the adiabatic approximation [5]), the frozen configuration assumption [5, 8]). Up to now antisymmetrization effects [6, 7]), the role of the relative motion between the two nuclei [5, 6, 9]) and mutual polarization effects [4, 7]) have been discussed. While the more elaborate methods of refs. [2–5]) are limited to symmetric and not too heavy systems (up to $^{40}Ca+^{40}Ca$) due to numerical difficulties, the methods where the single particle densities do not change during the collision [5–8]) can easily be extended to any pair of nuclei. A problem which arises in the latter case is to find an adequate approximation to the kinetic energy density.

The purpose of this paper is twofold. The first is to look for an improvement to the Thomas-Fermi approximation to the kinetic energy density which was used in earlier work [8]). The second is to study the validity of the proximity form of a nucleus-nucleus potential derived within the Skyrme interaction energy functional.

In sect. 2 we describe the kinetic energy approximation. We show its effect is to improve the calculated potential in the barrier region.

In sect. 3 we derive a proximity type form for our potential and discuss the importance of the curvature corrections. Sect. 4 is a summary of the results.

2. The kinetic energy approximation

We are calculating the real part of the nucleus-nucleus potential according to the formalism of ref. [8]). There the interaction potential between two nuclei 1 and 2 was defined as the integral

$$V(R) = \int [H(\rho, \tau) - H(\rho_1, \tau_1) - H(\rho_2, \tau_2)] \mathrm{d}\boldsymbol{r}, \tag{1}$$

where R is the separation distance between the centres of the interacting nuclei and $H(\rho, \tau)$ is the Skyrme interaction energy density [1]).

In ref. [8]) we have calculated the interaction potential between two nuclei in the sudden approximation, i.e. taking the density ρ of the composite system as the sum of individual densities ρ_1 and ρ_2. The kinetic energy density τ can be defined as

$$\tau = \sum_i |\nabla \psi_i|^2, \tag{2}$$

or as

$$\tau' = -\sum_i \psi_i^* \nabla^2 \psi_i, \tag{3}$$

where ψ_i are the wave functions of the occupied neutron or proton single particle states. The quantities (2) and (3) are related by $\tau = \tau' + \frac{1}{2}\nabla^2 \rho$.

In ref. [8]) we have shown that the Thomas-Fermi approximation,

$$\tau_{\mathrm{TF}} = \tfrac{3}{5}(3\pi^2)^{2/3} \rho^{5/3}, \tag{4}$$

is quite a reasonable approximation to τ' and we have used it for the description of both the composite system and individual kinetic energy densities. The effect of this approximation is to replace $H(\rho, \tau)$ by a function $\bar{H}(\rho)$ depending only on the density ρ.

Using (4) for the composite system has the advantage of including a large part of the exchange effects due to antisymmetrization between nuclei as compared to the case $\tau' = \tau_1' + \tau_2'$ where the antisymmetrization is switched off [6]).

According to Randrup [10]) one might expect the TF approximation to better reproduce the quantity $\frac{1}{2}(\tau + \tau')$ instead of τ'. For the Hartree-Fock densities used in the present section and calculated with the Skyrme interaction SIII [ref. [11])] this is the case only in the tail region where both τ_{TF} and $\frac{1}{2}(\tau + \tau')$ are positive while τ' is negative. An example is given in fig. 1.

The use of (4) for τ' or even for $\frac{1}{2}(\tau + \tau')$ does not give satisfactory results, producing a potential not deep enough at the barrier. That is why we investigate here another

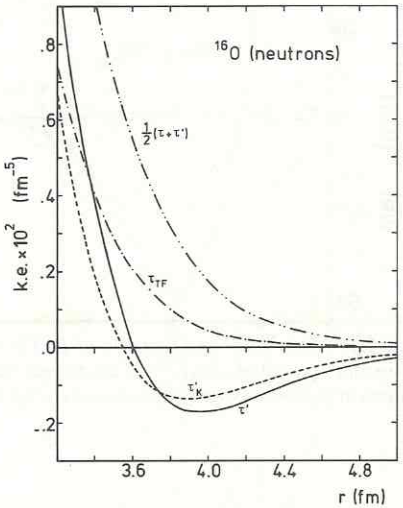

Fig. 1. The neutron k.e. density for ^{16}O: τ' – the exact k.e. density of eq. (3), τ_{TF} – the Thomas-Fermi approximation (eq. (4)), τ'_K – the Kirzhnits approximation (eq. (5)), $\frac{1}{2}(\tau+\tau')$ – an average density with τ and τ' from eqs. (2) and (3) respectively.

approximation to the k.e. density namely one due to Kirzhnits [12]) and others [see refs. [13, 14])]. This approximation consists in adding correction terms to τ_{TF} of eq. (4)

$$\tau'_K = \tau_{TF} + \tfrac{1}{36}(\nabla\rho)^2/\rho - \tfrac{1}{6}\nabla^2\rho. \tag{5}$$

The second term represents the Weizsäcker correction [15]). Fig. 1 shows a typical example of the validity of the approximation (5) in the k.e. density tail which is the significant region for the calculation of the potential around the barrier. One can see that τ'_K follows quite closely the exact density τ' of ^{16}O while τ_{TF} lies far above it. Expression (5) affects the terms in τ' and $\rho\tau'$ of the Skyrme interaction energy functional. The main change in the potential around the barrier comes from the pure k.e. term where only the Weizsäcker correction contributes.

Preliminary calculations showing the effect of using the eq. (5) for τ' were presented elsewhere [16]) for some specific pairs of nuclei. In this paper we preform calculations for all pairs of spherical nuclei. The characteristic shape of the potential is shown in fig. 2 for ^{90}Zr+^{208}Pb and the results are summarized in table 1. The part of the calculated potential between the inflexion point and the barrier was parametrized [8]) by a Saxon-Woods shape with parameters V_0, R_0 and T indicated in columns 2–4.

In column 5 there are the values V_N of the calculated potential at the barrier positioned at R_B (column 6). By comparison with table 3 of ref. [8]), one can notice that τ'_K produces a deeper potential and shifts the barrier position outwards by about 0.3 fm in each case. This means an increase of V_{calc}/V_{exp} at the strong absorption radius by a factor of 2 with respect to our previous calculations. But still from some of the existing experimental data it turns out that the ratio V_{calc}/V_{exp} is of the order 0.7–0.8. An example of the fit to experimental elastic scattering cross section for

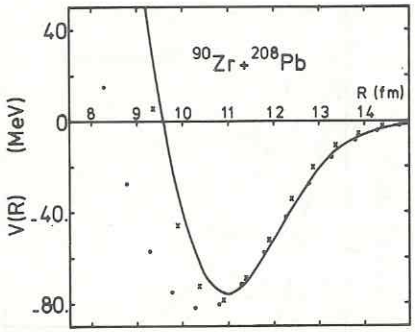

Fig. 2. The interaction potential for $^{90}Zr+^{208}Pb$ as a function of R. The full curve represents our exact result and the points are the proximity potential of ref. [18]). The crosses are the proximity approximation (eq. (7)) with our geometrical parameters and the values of $\varepsilon_0(S_0)$ from column 3 table 4.

TABLE 1

The nucleus-nucleus potential

Pair	$\bar{R}$ (fm)	V_0 (MeV)	R_0 (fm)	T (fm)	V_N (MeV)	R_B (fm)	γ (MeV/fm^2)	b (fm)
$^{16}O+^{16}O$	1.33	40.48	5.65	0.66	− 0.97	8.1	0.92	0.7981
$^{16}O+^{40}Ca$	1.55	46.93	6.80	0.658	− 2.14	8.8	0.91	
$^{16}O+^{48}Ca$	1.59	50.25	7	0.659	− 1.99	9.1	0.96	
$^{16}O+^{56}Ni$	1.63	99.82	7.25	0.648	− 2.71	9.1	0.94	
$^{16}O+^{90}Zr$	1.74	54.87	8.04	0.662	− 3.59	9.8	0.94	
$^{16}O+^{208}Pb$	1.91	61.87	9.8	0.675	− 5.31	11.4	0.95	
$^{40}Ca+^{40}Ca$	1.87	60.35	7.85	0.668	− 4.71	9.5	0.95	0.8525
$^{40}Ca+^{48}Ca$	1.93	69.1	8.07	0.668	− 4.47	9.8	0.99	
$^{40}Ca+^{56}Ni$	1.98	64.49	8.3	0.661	− 6.02	9.8	0.98	
$^{40}Ca+^{90}Zr$	2.15	71.74	9.1	0.672	− 7.95	10.5	0.99	
$^{40}Ca+^{208}Pb$	2.42	86.1	10.81	0.696	−13.19	12	1.02	
$^{48}Ca+^{48}Ca$	1.99	61.32	8.32	0.656	− 3.81	10.1	0.93	0.8525
$^{48}Ca+^{56}Ni$	2.04	69.75	8.5	0.663	− 5.73	10.1	1.02	
$^{48}Ca+^{90}Zr$	2.23	71.55	9.34	0.666	− 7.18	10.8	0.96	
$^{48}Ca+^{208}Pb$	2.51	80.31	11.07	0.679	−12.76	12.2	0.94	
$^{56}Ni+^{56}Ni$	2.10	67.59	8.78	0.646	− 7.75	10.1	0.99	0.8525
$^{56}Ni+^{90}Zr$	2.29	76.66	9.56	0.663	−10.21	10.8	1.00	
$^{56}Ni+^{208}Pb$	2.60	92.02	11.28	0.684	−19.02	12.2	1.03	
$^{90}Zr+^{90}Zr$	2.53	84.16	10.35	0.676	−14.69	11.4	0.99	0.8525
$^{90}Zr+^{208}Pb$	2.91	97.43	12.09	0.687	−28.40	12.7	0.96	
$^{208}Pb+^{208}Pb$	3.42	105.45	13.9	0.667			0.92	0.8888

Column 1: the reduced radius $\bar{R} = R_1R_2/(R_1+R_2)$. Columns 2–4: parameters of Saxon-Woods potentials V_0, R_0 and T_0 which approximate the tail of calculated potentials. Columns 5, 6: the value of the nuclear potential V_N at the barrier and the position of the barrier R_B. Column 7: the surface energy coefficient γ. Column 8: surface diffuseness b of a member of the interacting pair described by a Fermi-type density distribution.

$^{16}O+^{48}Ca$ at $E_{lab} = 40$ MeV where a discrepancy of about 2° in the critical angle still remains is shown in fig. 3.

As we have mentioned, the potential of the interacting pairs has a characteristic shape for all nuclei, with a repulsive core at short distances followed by an attractive pocket and a Woods-Saxon tail at larger distances. On the other hand the values taken by the potential seem to be related to the dimensions of the interacting nuclei.

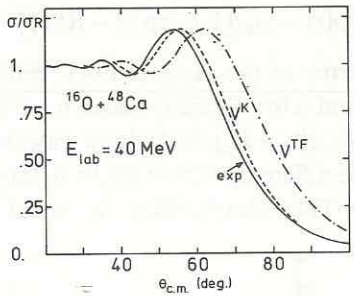

Fig. 3. The elastic scattering cross section σ/σ_R as a function of $\theta_{c.m.}$ for $^{16}O+^{48}Ca$ at $E_{lab} = 40$ MeV. The three curves are obtained with the phenomenological potential of ref. [17]) (solid), the present potential V^K (dashed) and the potential V^{TF} of ref. [8]) (dot-dashed) respectively.

It is therefore interesting to see if a mass (and consequently a size) dependence of the potential can be found. We end this section by showing the mass dependence of Woods-Saxon parameterization of the tail. In the next section we analyse the size dependence of the potential via the proximity concept.

By plotting V_0/D as a function of $D = A_1^{\frac{2}{3}}+A_2^{\frac{2}{3}}-(A_1+A_2)^{\frac{2}{3}}$ and R_0 and T as a function of $A_1^{\frac{1}{3}}+A_2^{\frac{1}{3}}$ we found an average dependence of these parameters on the masses A_1 and A_2 of the colliding nuclei, given by the following equations

$$\bar{V}_0/D = 15.76-0.63D,$$
$$\bar{R}_0 = 1.15(A_1^{\frac{1}{3}}+A_2^{\frac{1}{3}}), \tag{6}$$
$$\bar{T} = 0.644+0.003(A_1^{\frac{1}{3}}+A_2^{\frac{1}{3}}).$$

For $\bar{T}$ and $\bar{V}_0/D$ a change is noticed with respect to the results of ref. [8]). The dependence of $\bar{T}$ on $A_1^{\frac{1}{3}}+A_2^{\frac{1}{3}}$ is much slower, almost constant, and T is larger in all cases. Larger values of V_0 are also found but $\bar{V}_0/D$ decreases somewhat faster with D. The value of $\bar{R}_0$ remains practically the same.

3. Proximity potentials

According to Błocki *et al.* [18]) the interaction energy $V(R)$ of two nuclei with radii R_1 and R_2 whose centers are separated by a distance $R = R_1+R_2+S_0$ is given by

$$V(R) = 2\pi\frac{R_1R_2}{R_1+R_2}\int_{S_0}^{\infty} e(s)\mathrm{d}s. \tag{7}$$

In this equation $e(s)$ is a universal function which is the same for all pairs of interacting nuclei. It is the interaction energy per unit area of two plane semi-infinite sheets of nuclear matter with parallel surfaces separated by a distance S_0. In this section we reduce our potential (1) to the proximity form (7) and investigate the validity of the approximations which have to be made.

In this section we deal with Fermi density distributions

$$\rho(r) = \rho_0/[1+\exp((r-R)/a)], \tag{8}$$

which are parametrized forms of the Hartree-Fock densities used in the previous section. Parameters ρ_0, R and a for different nuclei have been given in ref. [8]). Values of $V(R)/\bar{R}$ where $\bar{R} = R_1R_2/(R_1+R_2)$ have been calculated for several values of surface separation S_0 for the different pairs of nuclei in table 1 and the corresponding points are plotted in fig. 4. They clearly show the trend of a universal function as

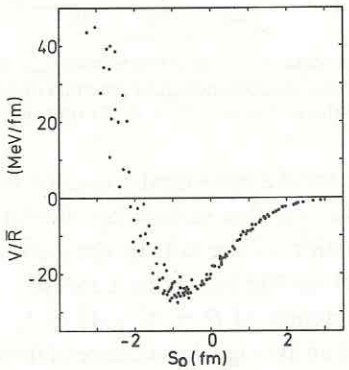

Fig. 4. The universal function extracted from the calculated potential V. The points $V/\bar{R}$ where $\bar{R} = R_1R_2/(R_1+R_2)$ are plotted against the separation distance S_0.

required by the proximity form (7). There are some deviations when the nuclei overlap, light pairs tending to give a repulsion with a larger radius. A similar graph has been presented by Ngô *et al.* [19]) for potentials calculated with Brueckner's energy density formalism. Taking into account their different scaling it turns out that our potentials are slightly less deep and have a narrower attractive pocket due to a thicker core.

The first step in the reduction of our potential to the proximity form is to replace the integrand in eq. (1) by a universal function

$$\bar{H}(\rho_1+\rho_2)-\bar{H}(\rho_1)-\bar{H}(\rho_2) = F(r_1-R_1, r_2-R_2) \tag{9}$$

depending on the distances r_1 and r_2 of the integration point P from the centers of the interacting nuclei (fig. 5). This replacement involves two approximations.

(a) The central density ρ_0 and surface diffuseness parameter a in eq. (8) must be the same for all pairs of nuclei. Only the half-density radii R_1 and R_2 change. Table 2 of ref. [8]) shows that there are variations of ρ_0 and a from light to heavy nuclei. The

consequences of these differences are discussed later in the section and their effects are illustrated in table 4.

(b) The integrand in eq. (1) contains terms like $\rho_1\rho_2$, $\rho_1\rho_2^2+\rho_2\rho_1^2$ when $\bar{H}(\rho)$ is derived from Skyrme's interaction. These terms have the form required by eq. (9). There are also terms proportional to

$$\nabla\rho_1 \cdot \nabla\rho_2 = \frac{\mathrm{d}\rho_1}{\mathrm{d}r_1}\frac{\mathrm{d}\rho_2}{\mathrm{d}r_2}\cos\theta_{12}, \tag{10}$$

where θ_{12} is the angle between r_1 and r_2 (fig. 5). The term (10) has the form required by eq. (9) if $\cos\theta_{12}$ is approximated by -1. This approximation should be reasonable if the main contribution to the integral (1) comes from a region of limited extent located between the two nuclei. The effect of this approximation for $^{208}\mathrm{Pb}+^{208}\mathrm{Pb}$ and $^{16}\mathrm{O}+^{16}\mathrm{O}$ is shown in tables 2 and 3. The potential V_{ex} is calculated by exact numerical integration of eq. (1) while V_2 is calculated by numerical integration with the approximation $\cos\theta_{12} \approx -1$ in terms like (10). The effect of the approximation is to increase the attraction especially for smaller values of R (negative values of $S_0 = R-R_1-R_2$). Surprisingly, for $S_0 > 0$ the extra attraction brought in by this approximation is practically independent of S_0, i.e. V_{ex}/V_2 is constant with respect to S_0.

After substituting eq. (9) into eq. (1) the integral can be reduced to a two-dimensional

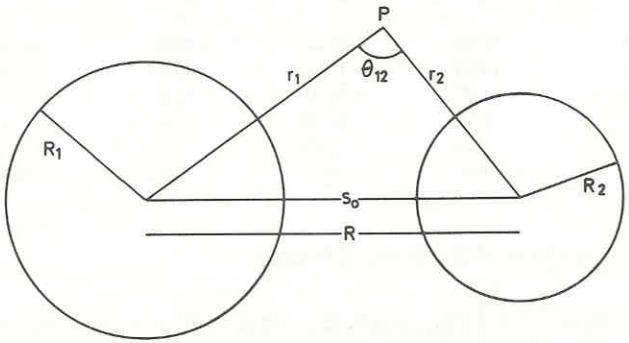

Fig. 5. The geometry of the system. P is the integration point, R the distance between centres, S_0 the separation between surfaces, R_1 and R_2 are the half-density radii of the interacting nuclei.

integral over r_1 and r_2 by making a change of variables

$$V(R) = \frac{2\pi}{R}\int\int F(r_1-R_1, r_2-R_2)r_1r_2\mathrm{d}r_1\mathrm{d}r_2. \tag{11}$$

The limits of integration are fixed by the triangular conditions

$$r_1+r_2 \geqq R, \qquad |r_1-r_2| \leqq R. \tag{12}$$

In the cases considered here the two radii R_1 and R_2 are much greater than the

surface diffuseness parameter a (i.e. the nuclei are leptodermous systems [18])]. As a consequence the integration limits can be extended by relaxing the restriction $|r_1-r_2| \leqq R$. Numerical calculations show that expanding the region of integration in this way gives a negligible error. This can be seen by comparing the columns V_{ex} and V_3 of each of the tables 2 and 3.

TABLE 2

Values of the potential for ^{208}Pb+^{208}Pb as a function of separation S_0 between the surfaces

S_0	R	V_p	V_1	V_2	V_3	V_{ex}
−2	11.664	−53.77	− 81.82	− 79.89	−46.92	−46.66
−1	12.664	−92.23	−106.12	−105.98	−87.53	−87.54
0	13.664	−61.45	− 70.12	− 69.89	−61.93	−61.93
1	14.664	−23.74	− 27.78	− 27.93	−25.34	−25.35
2	15.664	− 6.44	− 7.70	− 7.83	− 7.15	− 7.15
3	16.664	− 1.44	− 1.81	− 1.88	− 1.70	− 1.71

R is the separation between the centres $R = S_0+2R_1$ where R_1 is the half-density radius for Pb; V_p, V_1, V_2, V_3 are approximations, explained in the text. V_{ex} is the exactly calculated potential.

TABLE 3

Values of the potential for ^{16}O+^{16}O (as in table 2)

S_0	R	V_p	V_1	V_2	V_3	V_{ex}
−2	3.308	11.89	−34.46	−29.06	19.32	19.18
−1	4.308	−30.69	−47.36	−46.14	−22.31	−22.32
0	5.308	−24.17	−32.31	−32.09	−23.07	−23.17
1	6.308	− 8.59	−11.78	−12.13	− 9.68	− 9.68
2	7.308	− 1.94	− 2.80	− 3.03	− 2.50	− 2.50
3	8.308	− 0.38	− 0.57	− 0.66	− 0.54	− 0.54

Another change of variables in eq. (11) gives

$$V_2(R) = \frac{2\pi}{R}\int\int F(u_1, u_2)(R_1R_2+R_1u_2+R_2u_1+u_1u_2)\mathrm{d}u_1\mathrm{d}u_2, \tag{13}$$

with $u_1+u_2 > S_0$. We now make two further approximations:

(c) we assume that $S_0 \ll R_1+R_2$ so that $R \approx R_1+R_2$ and

(d) we neglect $R_1u_2+R_2u_1+u_1u_2$ in comparison with R_1R_2 in eq. (13).

Then we get an equation for $V(R)$ which has exactly the proximity form of eq. (7) with

$$e(s) = \int_{-\infty}^{\infty} F(u_1, s-u_1)\mathrm{d}u_1. \tag{14}$$

Values of $V_p(R)$ for ^{208}Pb+^{208}Pb and ^{16}O+^{16}O with $e(s)$ calculated from eq. (14) are shown in tables 2 and 3 respectively.

There is another, much less drastic, approximation for $V(R)$ which can be obtained from eq. (13) by neglecting only the term $u_1 u_2$ in the integrand. This gives

$$V_1(R) = 2\pi \frac{R_1 R_2}{R}\left[\varepsilon_0(S_0) + \frac{R_1+R_2}{2R_1R_2}\varepsilon_1(S_0)\right], \tag{15}$$

where

$$\varepsilon_n(S_0) = \int_{S_0}^{\infty} s^n e(s)\mathrm{d}s. \tag{16}$$

According to ref. [18]) the form (7) holds for the interaction of gently curved objects in close proximity. Eq. (15) includes the next corrections for finite curvature. It is also interesting because the correction can still be expressed in terms of the same function $e(s)$ which comes into the simple proximity formula.

Values of $V_1(R)$ for ^{208}Pb+^{208}Pb and ^{16}O+^{16}O are shown in tables 2 and 3 respectively. The numbers given in these tables show that V_1 (eq. (15)) and V_2 (eq. (13)) are very similar over a wide range of values of S_0. The differences between them is due to the term $u_1 u_2$ in eq. (13) which gives a small contribution. The larger corrections to the proximity form V_p are associated with the differences between V_1 and V_p and between V_{ex} and V_2. The quantity $V_1 - V_p$ is a curvature correction represented by the second term in eq. (15) and by the denominator R in eq. (15) which replaces R_1+R_2 in eq. (7). The difference between V_{ex} and V_2 is a result of the approximation $\cos\theta_{12} \approx -1$ in the surface terms (10) of the energy density. This is itself essentially also a curvature correction and clearly becomes smaller when the surfaces are very gently curved, as can be seen by comparing $V_{ex} - V_2$ for the cases ^{16}O+^{16}O and ^{208}Pb+^{208}Pb. The two corrections tend to cancel especially for small separation distances and this is the reason why V_p seems to be a good approximation to V_{ex} for smaller separations $|S_0| \lesssim 1$ fm. In the tail region ($S_0 \approx 3$ fm) curvature corrections are more important and the proximity form gives much less attraction than V_{ex}.

In relation to the discussion in the previous paragraph there is a comment which can be made about the proximity form of a folding type potential [cf. ref. [20])]. Such a potential has no surface terms (9) and the cancellation of different curvature corrections does not occur. Hence the proximity form, eq. (7), should be a less accurate approximation than in the present case or in the case considered in refs. [18,19]).

It remains to discuss the effects of approximation (a). The energy function $e(s)$ given by eq. (14) depends on the central density ρ_0 and the surface diffuseness a of the matter density of each of the interacting nuclei. Thus $e(s)$ is a universal function, the same for all pairs only if ρ_0 and a do not vary from nucleus to nucleus. There is in fact a significant variation between light and heavy nuclei and to gauge its effect we give in table 4 values of $\varepsilon_0(s)$ and $\varepsilon_1(s)$ (eq. (16)) calculated with the density parameters for ^{16}O and ^{208}Pb. Comparing the values of $\varepsilon_0(s)$ one can see that the parameters for ^{16}O give more repulsion at shorter separations i.e. for $S_0 < -1$ fm. This difference accounts for some of the spread of the points in fig. 4 for negative values of S_0.

TABLE 4

Comparison between momenta ε_0 and ε_1 of $^{16}O+^{16}O$ and $^{208}Pb+^{208}Pb$

S_0	$^{16}O+^{16}O$		$^{208}Pb+^{208}Pb$		Ref. [18])	
	ε_0	ε_1	ε_0	ε_1	$2\phi_0$	$2\phi_1$
2	1.426	−10.621	−2.505	−5.117	−4.651	−4.118
−1	−3.681	− 2.467	−4.297	−1.949	−4.969	−3.452
0	−2.899	− 2.593	−2.863	−2.760	−3.563	−4.061
1	−1.030	− 1.724	−1.106	−1.936	−1.719	−3.158
2	−0.233	− 0.609	−0.295	−0.794	−0.539	−1.465
3	−0.045	− 0.163	−0.067	−0.247	−0.135	−0.501

The last two column give the values of $2\phi_0$ and $2\phi_1$ of ref. [18]) to be compared to our results.

The last two columns of table 4 show the first and second incomplete moments of the universal function $\phi(S_0/b)$ of ref. [18]); these functions are given in terms of dimensionless variables, but the function $2\gamma\phi_0(S_0/b)$, where γ is a surface energy coefficient and b is a surface diffuseness parameter, corresponds to our $\varepsilon_0(S_0)$. In ref. [18]) the values $b = 1$ fm and $\gamma \approx 1$ MeV · fm^{-2} are used, and with these parameters values of ε_0 and $2\phi_0$ can be compared directly. We also show an example of a comparison of the proximity potential calculated in two versions for $^{90}Zr+^{208}Pb$ in fig. 2. The points represent the proximity potential derived from the universal function of ref. [18]) with parameters $b = 1$ fm, $\gamma = 0.9$ MeV · fm^{-2} and $R_1+R_2 = 11.78$ fm recommended in that reference. The solid curve is V_{ex} calculated from our energy functional eq. (1). The crosses are the proximity approximation (eq. (7)) to V_{ex} calculated with $\varepsilon_0(S_0)$ from the third column of table 4 ($R_1+R_2 = 11.89$ fm). The potential from ref. [18]) is qualitatively similar to our V_{ex}. It is somewhat more attractive especially in the surface region $R \gtrsim 13$ fm and for small separations $R \lesssim 11$ fm.

This picture emphasises that starting from values of the zeroth moment as different as $\varepsilon_0(S_0)$ and $2\gamma\phi_0(S_0/b)$ (table 4) for $S_0 > 0$ one can end up with potentials which look very similar. This is possible because the potentials vary very rapidly with separation distance so that even small changes in the radii R_1 and R_2 of the interacting nuclei can produce large changes in the potential. In the example shown in fig. 2 the small difference of 0.11 fm in R_1+R_2 compensates partly for the weaker attraction of $\varepsilon_0(S_0)$ as compared with $2\gamma\phi_0(S_0/b)$. For large values of S_0 the potentials are small and differences even as much as a factor of two cannot be distinguished on the diagram because of the scale.

The work of Błocki *et al.* [18]) makes a simple prediction about the maximum force F_m acting between two nuclei:

$$F_m = -4\pi\gamma \frac{R_1 R_2}{R_1+R_2}, \tag{17}$$

where γ is the surface energy coefficient of nuclear matter. We have extracted values of γ from our Saxon-Woods fits to the tails of potentials calculated from eq. (1). These are given in column 7 of table 1. The calculations give values of γ ranging from 0.91 MeV $\cdot$ fm^{-2} for ^{16}O + ^{40}Ca to 1.03 MeV $\cdot$ fm^{-2} for ^{56}Ni + ^{208}Pb with an average over all pairs of 0.97 MeV $\cdot$ fm^{-2}. This is near the nuclear matter value $\gamma \approx 1$ MeV $\cdot$ fm^{-2}. It is also possible to extract values of the parameter b using the definition in refs. [18,21]). These are given in the last column of table 1. These values of b are smaller than the value $b = 1$ fm and nearer the value $b = 0.872$ fm calculated from the Seyler-Blanchard interaction [22]) used in ref. [18]). Potentials obtained from the universal function of ref. [18]) depend on $\xi = S_0/b$. Choosing a value of b smaller than 1 fm would give a closer agreement between our results and those of ref. [18]).

4. Summary

We have presented results for the real part of the nucleus-nucleus potential calculated from a formalism based on Skyrme's interaction. Earlier calculations [8]) have been improved by using a more adequate approximation of the kinetic energy density in the tail region and consequently we have obtained a better description of the potential in the barrier region.

In the second part of our work we checked the validity of the proximity concept [18]) in our model. We wrote an expression for our potential as a sum of terms. One term has the proximity form of ref. [18]) except for a small difference in the denominator. Other terms give curvature corrections [eqs. (13), (15)]. There are two origins for the curvature corrections and a numerical study showed that they almost cancel for $S_0 \approx 0$ but increase for larger values of $|S_0|$. The error in the proximity approximation in the barrier region varies between 20 % for lighter pairs of nuclei to less than 10 % for heavier pairs.

Besides this study of the proximity approximation we have made a direct comparison of our potential with the proximity potential of ref. [18]) and have found them to be similar for separation distances $S_0 > 0$.

The differences between the proximity and our potential for $S_0 < 0$ might be attributed to the saturation properties of the two-body interaction used in each case.

The similarity with the proximity potential might originate from common features of both models: a two-body interaction which provides good binding energies, the frozen configuration assumption for the matter density, and the approximate description of the k.e. density. As the proximity theorem reduces the problem of the interaction between two finite nuclei to a simpler one, that of the interaction between two flat parallel slabs of semi-infinite nuclear matter it would be interesting to calculate the latter with better approximations.

One of us (F.S.) would like to thank Dr. P. E. Hodgson for kind hospitality offered to her at the Nuclear Physics Department in Oxford.

References

1) D. Vautherin and D. M. Brink, Phys. Rev. **C5** (1972) 626
2) K. H. Paessler *et al.*, Phys. Lett. **47B** (1973) 419
3) H. Flocard, Phys. Lett. **49B** (1974) 129
4) P. G. Zint and U. Mosel, Phys. Rev. **C14** (1976) 1488
5) G.-H. Göritz and U. Mosel, Z. Phys. **A277** (1976) 243
6) D. M. Brink and Fl. Stancu, Nucl. Phys. **A243** (1975) 175
7) J. Fleckner and U. Mosel, Nucl. Phys. **A277** (1977) 170
8) Fl. Stancu and D. M. Brink, Nucl. Phys. **A270** (1976) 236
9) S. A. Moszkowski, preprint, University of California, Los Angeles, 1977
10) J. Randrup, Nucl. Phys. **A259** (1976) 253
11) M. Beiner *et al.*, Nucl. Phys. **A238** (1975) 29
12) D. A. Kirzhnits, Field theoretical methods in many-body systems (Pergamon, Oxford, 1967) p. 52
13) C. Y. Wong, Phys. Lett. **63B** (1976) 395
14) O. Bohigas *et al.*, Phys. Lett. **64B** (1976) 381
15) C. F. v. Weizsäcker, Z. Phys. **96** (1935) 431
16) Fl. Stancu, Proc. Int. Workshop on Gross properties of nuclei and nuclear excitations V, Hirschegg, Jan 1977, ed. W. D. Myers
17) K. O. Groeneweld *et al.*, Phys. Rev. **C6** (1972) 805
18) J. Błocki, J. Randrup, W. J. Swiatecki and C. F. Tsang, LBL-5014 preprint, 1976
19) C. Ngô et al., Nucl. Phys. **A252** (1975) 237
20) D. M. Brink, Proc. European Conference on nuclear physics with heavy ions, Caen (France) 1976, J. de Phys. **37** (1976) C5;
    D. M. Brink and N. Rowley, Nucl. Phys. **A219** (1974) 79
21) W. D. Myers, Nucl. Phys. **A204** (1973) 465
22) R. G. Seyler and C. H. Blanchard, Phys. Rev. **124** (1961) 227; **131** (1963) 355